MOLECULAR ECOLOGY

Molecular Ecology (2017) **26**, 1386–1400 doi: 10.1111/mec.14013

Isolation with asymmetric gene flow during the nonsynchronous divergence of dry forest birds

JESSICA A. OSWALD,*† ISAAC OVERCAST,‡ WILLIAM M. MAUCK III,§ MICHAEL J. ANDERSEN§¶ and BRIAN TILSTON SMITH§

*Florida Museum of Natural History, University of Florida, Gainesville, FL 32611-7800, USA, †Museum of Natural Science, Louisiana State University, 119 Foster Hall, Baton Rouge, LA 70803, USA, ‡Subprogram in Ecology, Evolution and Behavior, The Graduate Center of the City University of New York, New York, NY 10016 USA, §Department of Ornithology, American Museum of Natural History, Central Park West at 79th Street, New York, NY 10024, USA, ¶Department of Biology and Museum of Southwestern Biology, University of New Mexico, Albuquerque, NM 87131, USA

Abstract

Dry forest bird communities in South America are often fragmented by intervening mountains and rainforests, generating high local endemism. The historical assembly of dry forest communities likely results from dynamic processes linked to numerous population histories among codistributed species. Nevertheless, species may diversify in the same way through time if landscape and environmental features, or species ecologies, similarly structure populations. Here we tested whether six co-distributed taxon pairs that occur in the dry forests of the Tumbes and Marañón Valley of northwestern South America show concordant patterns and modes of diversification. We employed a genome reduction technique, double-digest restriction site-associated DNA sequencing, and obtained 4407–7186 genomewide SNPs. We estimated demographic history in each taxon pair and inferred that all pairs had the same best-fit demographic model: isolation with asymmetric gene flow from the Tumbes into the Marañón Valley, suggesting a common diversification mode. Overall, we also observed congruence in effective population size (N_e) patterns where ancestral N_e were 2.9–11.0× larger than present-day Marañón Valley populations and 0.3–2.0× larger than Tumbesian populations. Present-day Marañón Valley N_e was smaller than Tumbes. In contrast, we found simultaneous population isolation due to a single event to be unlikely as taxon pairs diverged over an extended period of time (0.1–2.9 Ma) with multiple nonoverlapping divergence periods. Our results show that even when populations of codistributed species asynchronously diverge, the mode of their differentiation can remain conserved over millions of years. Divergence by allopatric isolation due to barrier formation does not explain the mode of differentiation between these two bird assemblages; rather, migration of individuals occurred before and after geographic isolation.

Keywords: coalescent, model selection, neotropical, phylogeography, South America, speciation with gene flow

Received 13 September 2016; revision received 30 November 2016; accepted 29 December 2016

Introduction

Populations are subject to fluctuations in habitat availability, connectivity to other areas and fragmentation. Over evolutionary time frames, these dynamics result in changes to genetic diversity, population differentiation and rates of gene flow (Avise 2000). Strong landscape and climatic changes may induce a synchronous evolutionary response in a community of species (e.g. Hickerson *et al.* 2006), but variation in when species originate within a community and their ecological ability to respond to changing conditions can produce an array of population histories (e.g. Smith *et al.* 2014b).

Correspondence: Jessica A. Oswald, Fax: +1 352 846 0287; E-mail: oswaldj3@gmail.com

Given this expected variance, a shared demographic history among codistributed species may be unlikely. However, species may show the same modes of diversification if landscape features, climatic cycles and/or species ecology act similarly on structuring populations during different time periods. In many groups of organisms, allopatric differentiation is the presumed dominant mode of diversification (Mayr 1963), but increasing evidence suggests that isolation with gene flow is also a common mechanism (Pinho & Hey 2010). Understanding the degree of congruence in both modes and patterns of diversification will help explain how complex interactions between environment and species biology affect population history.

Comparative phylogeographic studies typically assess similarity along one axis of genetic variation. This approach often entails testing for congruence in a parameter of interest, such as phylogeographic breaks (Satler & Carstens 2016), divergence times (Myers *et al.* 2016) or demographic expansions (Burbrink *et al.* 2016; Prates *et al.* 2016). Although population genetic parameters are not necessarily independent of one another, a process such as habitat change, for example, could affect population size but not fragmentation. This phenomenon is often observed in studies that show a high degree of concordance in the location, but not the depth, of phylogeographic breaks (e.g. Smith *et al.* 2014b). Thus, testing whether populations have a shared history is more robust when multiple aspects of genetic variation can be compared across codistributed species. Developments in model-based phylogeography (Hickerson *et al.* 2010) and the relative ease of acquiring genome-wide genetic markers (McCormack *et al.* 2013) now provide the means of expanding hypothesis testing beyond a simple dichotomy of concordance or discordance. These advancements are particularly relevant for taxa inhabiting complex environments, such as those along topographic gradients, where multiple historical and biological processes underlie the demographic histories of a community.

In the tropical Americas, Pleistocene climatic cycling between cooler and drier glacial periods to warmer and wetter interglacial periods caused a reconfiguration of species distributions (Colinvaux *et al.* 1996, 2000; Cohen *et al.* 2014; Oswald & Steadman 2015). Under current climatic conditions, seasonally dry forests (hereafter dry forest) are discontinuous in inter-Andean valleys, lowland areas peripheral to the Amazon Basin, and along much of the Pacific coast from the west slope of the Andes to México (Pennington *et al.* 2006). The humid habitats that are found adjacent to these arid biomes are more continuously distributed. During the Pleistocene, many plant taxa in the Neotropical region experienced range expansions or contractions associated with climate fluctuations (Colinvaux *et al.* 1997, 2000). These dynamics are evident in the Quaternary animal fossil record (last 2.6 million years [Myr]), which shows fluctuations in the composition and distribution of some species now found in dry forest (Lemon & Churcher 1961; Campbell 1979, 1982; Pennington *et al.* 2000; Oswald & Steadman 2015). More expansive arid biomes would have allowed species in these regions to increase their population sizes and move more readily between areas via habitat corridors.

In northwestern South America, the western cordillera of the Andes separates two dry forests. To the west lies the Tumbesian region (hereafter Tumbes), which extends into Ecuador, and to the east lies the inter-Andean Marañón Valley (Fig. 1). The Andes in northern Peru and southern Ecuador only reach relatively low elevations in an area termed the Huancabamba Depression (Weigend 2002). The western Andean cordillera is continuous across this region but contains the lowest pass in the Central Andes, the Porculla Pass, at 2145 m (Weigend 2002; Bridgewater *et al.* 2003; Linares-Palomino *et al.* 2003; Linares-Palomino 2006). The Porculla Pass is a putative dispersal corridor between the Marañón Valley and Tumbes (Bridgewater *et al.* 2003). Currently, this pass sustains mesic montane vegetation (Bridgewater *et al.* 2003) and may serve as a dispersal barrier for arid-adapted taxa. However, Pleistocene climatic fluctuations may have facilitated the movement of dry forest plant species through Porculla Pass leading to the dispersal of other species, such as birds (Cadena *et al.* 2016). Within the Tumbes and the Marañón Valley, taxonomic assemblages show high community turnover (Stotz *et al.* 1996; Pennington *et al.* 2009; Linares-Palomino *et al.* 2010; Oswald *et al.* 2016) and high levels of species endemism, both in the region as a whole and within each subregion (e.g. 77 bird species; 124 plant species; Parker *et al.* 1995; Pennington *et al.* 2006; Stattersfield *et al.* 1998). Fossils indicate that dry forests have been in the region since at least 8–12 million years ago (Ma) (Burnham 1995; Burham & Graham 1999; Burnham & Carranco 2004; Pennington *et al.* 2006, 2009) and these plant communities have persisted through long-term isolation, in situ speciation, and niche conservatism (Pennington *et al.* 2009; Särkinen *et al.* 2012).

Multiple processes could explain how communities distributed across the western cordillera of the Andes became differentiated. The final uplift of the Andes may have fragmented the once more continuous habitat connecting the present-day Marañón Valley and Tumbes dry forests, which would leave congruent and deep (3–5 Ma) genetic divergences in the Pliocene among codistributed species. Pleistocene climatic cycles may have left a similar genetic signature in codistributed taxa, although congruent genetic divergences would be shallower, dating to within the last 2.6 Myr.

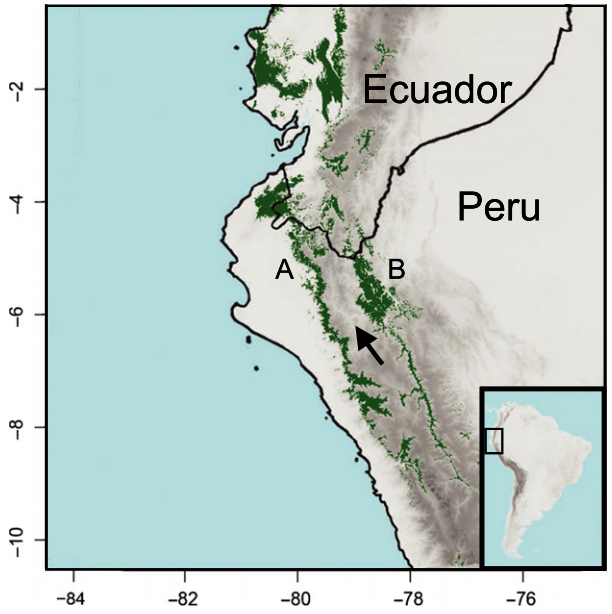

Fig. 1 The western Andean cordillera divides two tracts of dry forest (in green) in northwest Perú and southwest Ecuador. The distribution of dry forest in the region is based on Särkinen *et al.* (2011) and Bridgewater *et al.* (2003). The Tumbesian ('Tumbes') dry forests are found west of the Andes (a). East of the western cordillera, dry forests are found within the Marañón Valley (b). The lowest pass of the central Andes, Porculla Pass (at 2145 m; see arrow), is a putative corridor allowing for gene flow between Tumbes and the Marañón Valley. [Colour figure can be viewed at wileyonlinelibrary.com]

An alternative explanation to synchronous divergence caused by environmental and landscape change is isolation via long-distance dispersal, where species colonize an area and diversify across an extended period of time. These three scenarios implicitly assume diversification by allopatric speciation such that once populations become geographically isolated, they no longer exchange genes and begin to evolve independently. However, gene flow among areas could continue after geographic isolation and diversification could occur via divergence with gene flow (Pinho & Hey 2010). This movement of individuals after isolation could be random; alternatively, landscape features and ephemeral dispersal corridors, in conjunction with physiological constraints, could produce congruent patterns of gene flow (e.g. Cheviron & Brumfield 2009; DuBay & Witt 2014; Cadena *et al.* 2016). Distinguishing among these alternative hypotheses is possible by inferring the degree of congruence in diversification pattern and mode.

Here, we modelled the demographic history of six taxon pairs of birds that occur in the dry forests of Tumbes and the Marañón Valley in northwestern South America and assessed the degree of similarity in their population history and mode of diversification. We collected thousands of unlinked loci from individuals in populations from both areas using double-digest restriction site-associated DNA (*dd*RAD) sequencing. To model population history and estimate population genetic parameters from the *dd*RAD loci, we used both full- and composite-likelihood approaches that employed a coalescent model. First, we assessed whether divergence times were asynchronous as a result of protracted diversification, or synchronously correlated with either Late Pliocene Andean Uplift or Pleistocene glacial cycling. Second, we evaluated whether ancestral effective population sizes were larger than extant daughter populations, which would be consistent with formerly more expansive arid habitats that promoted larger ancestral populations. Third, we generated demographic models ranging from pure isolation to isolation with symmetric gene flow, and used model selection to identify the best fitting model in order to test whether the taxon pairs differentiated via a similar process.

Materials and methods

Taxon sampling

We selected six taxon pairs representative of the passerine diversity in the dry forests of northwestern South America, with our genetic sampling focused on Peru. Of the six pairs, five consisted of named subspecies pairs, whereas the sixth was a sister species pair. In each case, one member of the pair had the majority of its range in Tumbes or the Marañón Valley (Fig. 1). One exception was *Saltator striatipectus*, which contains multiple phylogeographic lineages that are distributed in northern South America and Central America (Chaves *et al.* 2013). The pairs were as follows, with the Marañón Valley taxon presented first followed by the Tumbesian taxon: *Thamnophilus bernardi shumbae – T. b. bernardi*; *Melanopareia maranonica – M. elegans*; *Campylorhynchus fasciatus fasciatus – C. f. pallescens*; *Mimus longicaudatus maranonicus – M. l. longicaudatus*; *Arremon abeillei nigriceps – A. a. abeillei; Saltator striatipectus peruvianus – S. s. immaculatus*. We included 9–14 individuals per population, all from vouchered specimens (Table S1, Supporting information). We also included one outgroup taxon that was sister to each pair (*Thamnophilus bridgesi*; *Melanopareia maximiliani*; *Campylorhynchus albobrunneus*; *Mimus saturninus*; *Arremon aurantiirostris*; *Saltator striatipectus* from Panama).

Double-digest restriction site-associated DNA sequencing

To obtain genome-wide genetic variation, we used double-digest restriction site-associated DNA sequencing

(*ddRAD*; Peterson *et al.* 2012) to produce reduced-representation libraries for our focal taxa. Briefly, we extracted genomic DNA from tissue using the DNeasy tissue extraction kit (Qiagen, Valencia, CA), quantified DNA extractions using a QUBIT 2.0 fluorometer, and then reconcentrated each sample to approximately 300 ng per 10.5 μL. Prior to digestion–ligation, we annealed phosphorylated and phosphorothioated adaptors to enable adaptor ligation simultaneously with restriction digestion. We digested each sample in two 96-well plates (72 samples per plate) using restriction enzymes SbfI-HF and MspI, and ligated one of the unique 6-bp P1 adapters to SbfI-HF and the universal MspI P2 adapter to DNA fragments. Digestion–ligation reactions contained 10× CutSmart, 4 μM P1 adapters, 4 μM P2 adapters, 10 mM ATP, 15 U SbfI-HF, 15 U MspI and 300 U T4 ligase; all enzymes were purchased from New England Biolabs (Ipswich, MA, USA).

We pooled uniquely barcoded digestion/ligation reactions within each index group (eight samples per pool from each column of the plate; nine pools per plate). Then, we performed an AMPure XP (1.5×) bead cleanup of each pool following manufacturer's protocol before gel size selecting a 250–500 bp range using an angled gel plug following DaCosta & Sorenson (2014). We extracted DNA from 2% agarose (1% low melt agarose + 1% normal agarose) gel plugs using a QIAquick Gel Extraction Kit (Qiagen, Valencia, CA). Next, we annealed one of the nine unique index primers using PCR (98 °C for 30 s, followed by 16 cycles of 98 °C for 5-s, 60 °C for 25 s, 72 °C for 30 s and a 72 °C final extension for 5 min). Each sample had a unique P1 adapter and index primer combination. We cleaned each amplified pool using AMPure beads and verified the size and quality of libraries using an AGILENT 2100 BIOANALYZER. The *dd*RAD libraries were sequenced at the New York Genome Center on two lanes of an Illumina HiSeq 2500 (paired-end 100 bp).

Assembly of ddRAD loci

To assemble de novo loci from raw *dd*RAD sequence data, we used PYRAD version 2.16.1 (Eaton 2014) and followed software guidelines for assembling loci from paired-end data, using default settings unless otherwise specified. First, we demultiplexed individual samples from raw fastq data based on index group and adapter sequence. Next, we filtered reads by converting bases with a Phred quality score <20 (amounting to 99% confidence in the base call) to ambiguous sites (N) and excluding reads with >4 ambiguous sites. We then clustered filtered reads within each sample using an 85% sequence similarity threshold. Next, we jointly inferred the error-rate and heterozygosity within samples and called consensus sequences for each *dd*RAD locus, excluding loci with more than two alleles as potential paralogs and requiring a minimum depth of coverage per locus of six. Finally, we clustered loci across samples at 85% sequence similarity, aligned sequences within clusters and filtered loci containing one or more sites that appeared heterozygous across more than three samples. We exported the final data set as SNPs and sequences in various formats. PYRAD also produced a summary of the data including number of variable sites, parsimony informative sites, SNPs and loci.

Genetic structure and variation

To assess the degree of genetic structuring among the Tumbes and Marañón populations, we used the population assignment approach implemented in STRUCTURE version 2.3.4 (Pritchard *et al.* 2000). STRUCTURE assigns individuals to a user-defined number of populations with assigned likelihood values for each data partition. We used 500 000 MCMC generations after an initial burn in of 10 000 generations with 10 replicates for each cluster (K) value of 1–5 for all taxon pairs. To evaluate likelihood scores for *K* values, generate input files for CLUMPP (Jakobsson & Rosenberg 2007) and combine STRUCTURE result files, we used Structure Harvester (Earl & vonHoldt 2012). Next, we combined STRUCTURE population assignments for each replicate with the full search algorithm implemented in CLUMPP (Jakobsson & Rosenberg 2007). Then, we produced STRUCTURE plots in R (R Core Team 2014) using the combined results matrix. Finally, we determined optimal *K* values based on likelihood scores and Δ*K* values (Evanno *et al.* 2005). We also visualized genetic structuring by plotting pairwise genetic distance matrices for each population pair using the Python Package SCIKIT-ALLEL (Miles & Harding 2016) as a heatmap, where warmer colours showed genetically dissimilar individuals and cooler colours showed genetically similar individuals. To further characterize genetic diversity, we calculated several summary statistics for each taxon pair and for each population within each taxon pair including nucleotide diversity (π), observed and expected heterozygosity (H_O/H_E), Watterson's Theta (θ_W), D_{xy} (an absolute measure of population differentiation) and Tajima's D. We performed these calculations using the SCIKIT-ALLEL package (Miles & Harding 2016).

We mapped filtered reads to the Zebra finch (*Taeniopygia guttata*) reference genome (Ensembl assembly number 3.2.4) using SMALT version 0.7.6 (http://www.sanger.ac.uk/science/tools/smalt-0) and SAMTOOLS version 1.3 (Li *et al.* 2009) to examine the distribution of *dd*RAD loci across an avian genome. Reference sequence mapping with SMALT is a two step process: the first step

indexes the reference genome, and the second step aligns reads to the reference sequence. To optimize settings for the indexing step, we tested several combinations of *wordlen* (-k) and *skipstep* (-s) values and identified that 16 for both maximized the number of reads successfully mapped. For the alignment step, we performed an exhaustive search (-x) for matches of each read to the reference. We tested values for sequence similarity (-y) between 0.8 and 0.95 and chose 0.85 in the final analyses because it was conservative without being overly restrictive. For each paired-end read, we aligned both reads simultaneously and only considered reads if both reads mapped successfully and were properly paired. As our focal taxa are widely dispersed across the avian tree of life, their phylogenetic distances from the Zebra Finch are quite disparate. Mean temporal distances between our taxon pairs and the Zebra Finch range from ~50 Myr (*Thamnophilus* and *Melanopareia*), ~36 Myr (*Campylorhynchus* and *Mimus*) and ~30 Myr (*Arremon* and *Saltator*) (Claramunt & Cracraft 2015). Because of the variation in phylogenetic distance between each focal taxon and the Zebra Finch, we expected to see a concordant reduction in the fraction of *dd*RAD loci that map successfully. Regardless, our primary interest was to test the homogeneous distribution of the reads, and we do not expect phylogenetic distance to have a substantial impact on our mapping results.

Demographic modelling

We implemented two separate approaches to model the demographic history of the six taxon pairs. One approach, G-PhoCS (Gronau *et al.* 2011), used a full-likelihood, multispecies coalescent model where the input data were the entire sequence for each *dd*RAD locus. The second approach, fastsimcoal2 (Excoffier *et al.* 2013), was a composite-likelihood method that simulated the expected joint site frequency spectrum (SFS) where the input data were a SFS produced from SNPs in the *dd*RAD loci. Because estimating the marginal likelihood in G-PhoCS has been shown to be unreliable, model comparison using Bayes Factors is not yet possible in the program (pers. comm. I. Gronau). Only the composite-likelihood method, fastsimcoal2, allowed us to test likelihood of the data given alternative demographic models, but we present G-PhoCS parameter estimates from both pure isolation and isolation with migration models. Using these two approaches, we assessed both the similarity and uncertainty in parameter estimates between methods.

G-PhoCS is based on the MCMCcoal model, which employs a multispecies coalescent framework to estimate divergence times and effective population sizes from multilocus sequence data (Yang 2002; Rannala & Yang 2003), but additionally allows for modelling gene flow between populations along user-defined migration bands (Gronau *et al.* 2011). We wrote a custom module to convert the alleles file output from PYRAD into the G-PhoCS format. We then estimated the timing of divergence (τ) between the Tumbes and Marañón Valley populations and the population mutation rate parameter for extant and ancestral lineages (θ) in models that allowed and disallowed migration. G-PhoCS uses gamma (α, β) distributions to specify the prior distributions for θ, τ and m_{sx}. These parameters are the population standardized mutation rate parameter ($\theta = 4N_e\mu$ for a diploid locus, where μ is mutations per nucleotide site per generation); the species divergence time parameter ($\tau = T\mu$; T = species divergence time in millions of years); and the migration rate per generation parameter ($m_{sx} \times \theta_x/4 = M_{sx}$), which is the proportion of individuals in population x that arrived by migration from population s per generation. We performed two sets of G-PhoCS analyses using different priors (τ–θ: ([prior 1: 1, 300] and [prior 2: 1, 30]) that represented shallow to deep phylogeographic divergences and smaller to larger θ values by changing the shape parameter (α) and scale parameter (β), which have a mean α/β and variance $s^2 = \alpha/\beta^2$. We ran pure isolation models and models with bidirectional gene flow. For the models that allowed migration, we specified a prior distribution of (1, 10) on the migration band. Posterior estimates of the migration rate from G-PhoCS are influenced by the prior distribution (e.g. Gronau *et al.* 2011; Smith *et al.* 2014a); thus, we include migration bands to assess how gene flow may have influenced other demographic parameters, but not as accurate estimates of migration. We converted G-PhoCS τ and θ estimates using the Zebra Finch genome-wide mutation rate (2.21×10^{-9} substitutions/site/year; Nam *et al.* 2010) assuming a generation time of 1 year. We ran each model multiple times for 500 000 generations, sampling every 100, and we performed MCMC diagnostics in TRACER version 1.6 (Rambaut & Drummond 2010).

We used a complimentary demographic approach by employing fastsimcoal2 (Excoffier *et al.* 2013) to obtain estimates of migration, explicitly test different demographic models and provide a comparison to G-PhocS parameter estimates. fastsimcoal2 uses coalescent simulations to model different demographic scenarios from the site frequency spectrum (SFS) from large multilocus data sets (Excoffier *et al.* 2013). We used a custom Python script to convert the VCF file from PYRAD into ∂a∂i format – a concise summary of the within and among population genetic diversity at biallelic sites (Gutenkunst *et al.* 2009) – and randomly selected one SNP per locus to reduce linkage bias. We then used

∂a∂i to create a folded joint SFS for each taxon pair. Because the SFS is calculated from a complete data matrix, ∂a∂i provides a function for averaging over missing data by projecting the full data set down to a smaller number of samples per population. We calculated and visualized all possible projections of the full SFS down to a range of values from 5 × 5 to 11 × 11 samples per population. We elected to project the SFS for all taxon pairs down to 8 × 8 samples, a resolution we found suitable to maximize the number of segregating sites comprising the SFS, following the recommendation of the ∂a∂i developers. We performed simulations using a two-population model that represented the Tumbes and Marañón Valley populations, and we varied the presence and direction of migration among models. For all models, we specified extant and ancestral effective population sizes (N_e) to have a prior range of 50 000–1 000 000 with a log uniform distribution and divergence time (TDIV) to have a prior range of 100 000–3 000 000 generations. Prior ranges for migration are specified below, and all ranges were log uniform converted. The isolation models were as follows: (M1) no migration (three free parameters), (M2) symmetric migration (four free parameters; M_{12}: 1×10^{-3} - 20), (M3) asymmetric migration (five free parameters; N_1M_1: 1×10^{-3} - 20; N_2M_2: 1×10^{-3} - 20), (M4) unidirectional migration (four free parameters; Marañón Valley to Tumbes; N_1M_1: 1×10^{-3} - 20) and (M5) unidirectional migration (four free parameters; Tumbes to Marañón Valley; N_1M_1: 1×10^{-3} - 20). For each set of simulations, we specified the sample sizes (Tumbes: $n = 9$; Marañón Valley: $n = 9$) to match the resolution of our SFS. We ran 100 000 simulations with 100 independent replicates for each model. To increase performance, we specified two cores per process with the runtime parameter '-c 2'. We then used an information theory approach for model selection (Burnham & Anderson 2003), which entailed estimating the ΔAIC, relative likelihood and AIC weight for each model, and selecting the best-fit model. For the best-fit model for each taxon pair, we performed 50 parametric bootstraps to produce mean and 95% confidence intervals for each parameter. Parameter values are presented as absolute values that were converted by fastsimcoal2 using the Zebra Finch genome-wide mutation rate (Nam *et al.* 2010).

Results

We collected thousands of loci and SNPs for six taxon (subspecies or species) pairs from 9–14 individuals per population that have distinct taxa in the Tumbes and Marañón Valley of northwestern South America (Table S1, Supporting information). For convenience, we will refer to these taxon pairs by their generic names: *Melanopareia*, *Thamnophilus*, *Campylorhynchus*, *Mimus*, *Arremon* and *Saltator*. See Materials and methods section for full details on taxonomy. We multiplexed 136 samples on two lanes of an Illumina HiSeq 2500. This produced an average of 12 654 clusters per sample with a mean coverage depth of 19× (SD = 76×) for all ingroup samples (except three that were omitted), where 46% of the clusters had a mean depth >5× (mean = 36×, SD = 104×). Excluding two additional samples that were removed, we obtained 14 739–49 866 variable sites, 6130–25 775 parsimony informative sites and 4407–7186 SNPs per taxon pair (Table 1). We also collected data from one outgroup per taxon pair with the number of loci varying from 4 to 2770. Given the variable success at sequencing outgroup taxa, we excluded outgroups from downstream analyses. In total, between 6 and 34% of reads were properly paired and successfully mapped to an annotated reference genome of the Zebra Finch (Fig. S1, Supporting information). The percentage of overall mapping success per taxon pair was qualitatively correlated with phylogenetic distance from the Zebra Finch. Of the reads that successfully mapped with their mate pair, on average 2.3% mapped to the Z chromosome, 0.1% to the mitochondrial genome, and 83.48% to autosomes and 14.21% to unplaced scaffolds (Fig. S1, Supporting information). There was a tendency for larger chromosomes to have fewer mapped reads, and smaller chromosomes to have more mapped reads given their size (Fig. S1, Supporting information).

We assessed the degree of genetic structure among the Tumbes and Marañón Valley populations and within population genetic variation. The number of SNPs used in STRUCTURE analysis for each taxon pair was as follows: *Thamnophilus*: $n = 5468$; *Melanopareia*: $n = 6385$; *Campylorhynchus*: $n = 4568$; *Mimus*: $n = 4407$;

Table 1 Summary of *dd*RAD loci for each taxon pair from PYRAD

Taxon pair	*n*	Var. sites	PSI	SNPs	Num. of loci
Thamnophilus	22	21 404	9606	5468	1049–4514
Melanopareia	17	37 296	18 794	6385	187–4728
Campylorhynchus	23	14 739	6130	4568	2091–4535
Mimus	22	18 933	8857	4407	206–3529
Arremon	19	34 161	15 421	5257	726–3510
Saltator	21	49 866	25 775	7186	1886–4840

Column names are as follows: *n*, sample size; Var. Sites, the total number of variable sites; PSI, the total number of parsimony informative sites; SNPs, the total number of single nucleotide polymorphisms; and Num. of Loci, the range of number of loci across the individuals in each taxon pair.

Arremon: n = 5255; *Saltator*: n = 7186 (Table 1). STRUCTURE analysis indicated that the most likely number of clusters was two (K = 2) for each taxon pair except for *Thamnophilus* and *Campylorhynchus*, which were best explained by three clusters (K = 3; Table S2; Figs 2, S3, Supporting information; see Fig. S2, Supporting information for museum Accession nos for each individual). Additionally, the average likelihood score and the highest ΔK value were not congruent across cluster values for *Saltator* (Table S2; Figs S2, S3, Supporting information). The poorer fit of *Thamnophilus* and *Campylorhynchus* to a two-population (Tumbes – Marañón Valley) model may be due to the shallow divergence of these taxon pairs, potentially gene flow from an unsampled population in Tumbes, or genetic drift (Falush *et al.* 2016). The degree of admixture varied across the taxon pairs, and we assessed these patterns in more detail in the demographic modelling section. Pairwise distance heatmap plots showed similar results as the STRUCTURE analysis, with clustering among the areas and with varying levels of admixture across the pairs (Fig. 3). In addition, the heatmaps further show that the Marañón Valley individuals are genetically more similar to each other than the Tumbes individuals are to each other (Fig. 3). Pairwise divergences per site (D_{xy}) were lower in *Campylorhynchus* (0.003), *Thamnophilus* (0.004) and *Mimus* (0.005) than *Saltator* (0.010), *Melanopareia* (0.010) or *Arremon* (0.009). Within populations in each area, π (mean = 0.004; SD = 0.001) and θ_W (mean = 0.005; SD = 0.002) were higher in the Tumbes populations and mean Tajima's D was higher in the Marañón Valley populations (mean = 0.094; SD = 0.114; Table 2).

Demographic modelling

Each G-PhoCS analysis took approximately 300–500 h per run (on a single Intel Core i7 3.4–4.0 GHz) to achieve sampling convergence, with the isolation with migration models taking longer. The number of unique loci used in both demographic analyses for each taxon pair was as follows: *Thamnophilus*: n = 7604; *Melanopareia*: n = 7133; *Campylorhynchus*: n = 6903; *Mimus*: n = 5620; *Arremon*: n = 5959; *Saltator*: n = 8195. For simplicity, we present G-PhoCS models with symmetric migration and prior 1 (τ–θ: [1, 300]) and present pure isolation model results elsewhere (Table S3, Supporting information). The G-PhoCS pure isolation and isolation with symmetric gene flow produced similar divergence times estimates and the parameter estimates were robust to the two priors we used (prior 1: τ–θ: [1, 300]; prior 2 τ–θ: [1, 30]). Mean divergence times ranged from 0.103 to 1.678 Ma and the 95% highest posterior densities spanned from 0.009 to 0.077 Ma (Fig. 4; Table S3, Supporting information). Ancestral population sizes were on average 5.1× and 2× higher than the Marañón Valley and Tumbes populations, respectively, and ranged from 0.495 to 1.550 million individuals. The 95% highest posterior densities for ancestral N_e spanned from 0.024 to 0.068 million individuals (Fig. 4; Table S3, Supporting information). The Tumbes population sizes (mean = 0.519 million individuals; SD = 0.278) averaged 2× larger than the Marañón Valley population sizes (mean = 0.253 million individuals; SD = 0.179; Table S3, Supporting information).

For fastsimcoal2, each model selection replicate took between 12 and 36 h (on a Nehalem 2.93 GHz CPU), depending on the number of parameters in the model. Total compute time, given that we ran 50 independent replicates for five different models for each of six taxon pairs, was approximately 36 000 h, with a wall-time of 1080 h. For all six taxon pairs, the best-fit demographic model was isolation with asymmetric migration. The relative likelihoods for the asymmetric migration models were 1.0 or near 1.0 in all cases, and the next most likely models were isolation with unidirectional or symmetric migration (Table 3). Mean divergence times ranged from 1.320 to 2.667 Ma, and the 95% confidence intervals obtained from the parametric bootstrapping spanned from 1.106 to 2.940 Ma (Fig. 4; Table S3, Supporting information). Ancestral N_e were on average 5.791 times higher than N_e in Marañón Valley populations, with means ranging from 0.574 to 0.904 million individuals and 95% confidence intervals spanning from 0.566–0.973 million individuals (Fig. 4; Table S3, Supporting information). In three of the taxon pairs, one daughter population (Tumbes) was larger than the ancestral population. The Tumbes N_e (mean = 0.623 million individuals; SD = 0.230) were an average 8.8× larger than the Marañón Valley N_e (mean = 0.075 million individuals; SD = 0.013). The migration rate from Tumbes into Marañón Valley across taxon pairs (0.225–0.762 individuals/generation) was 5.5–71.2× higher than from Marañón Valley into Tumbes (0.009–0.041 individuals/generation). (Table S3, Supporting information)

Discussion

In contrast to a traditional comparative model where codistributed species either evolve idiosyncratically or in concert, we inferred that populations of birds occurring in the dry forests of northwestern South America became isolated over a broad time frame but showed congruent modes of diversification. We found that populations differentiated between Tumbes and the Marañón Valley from 0.1 −2.9 Ma, which allowed us to reject a single mechanism as being responsible for

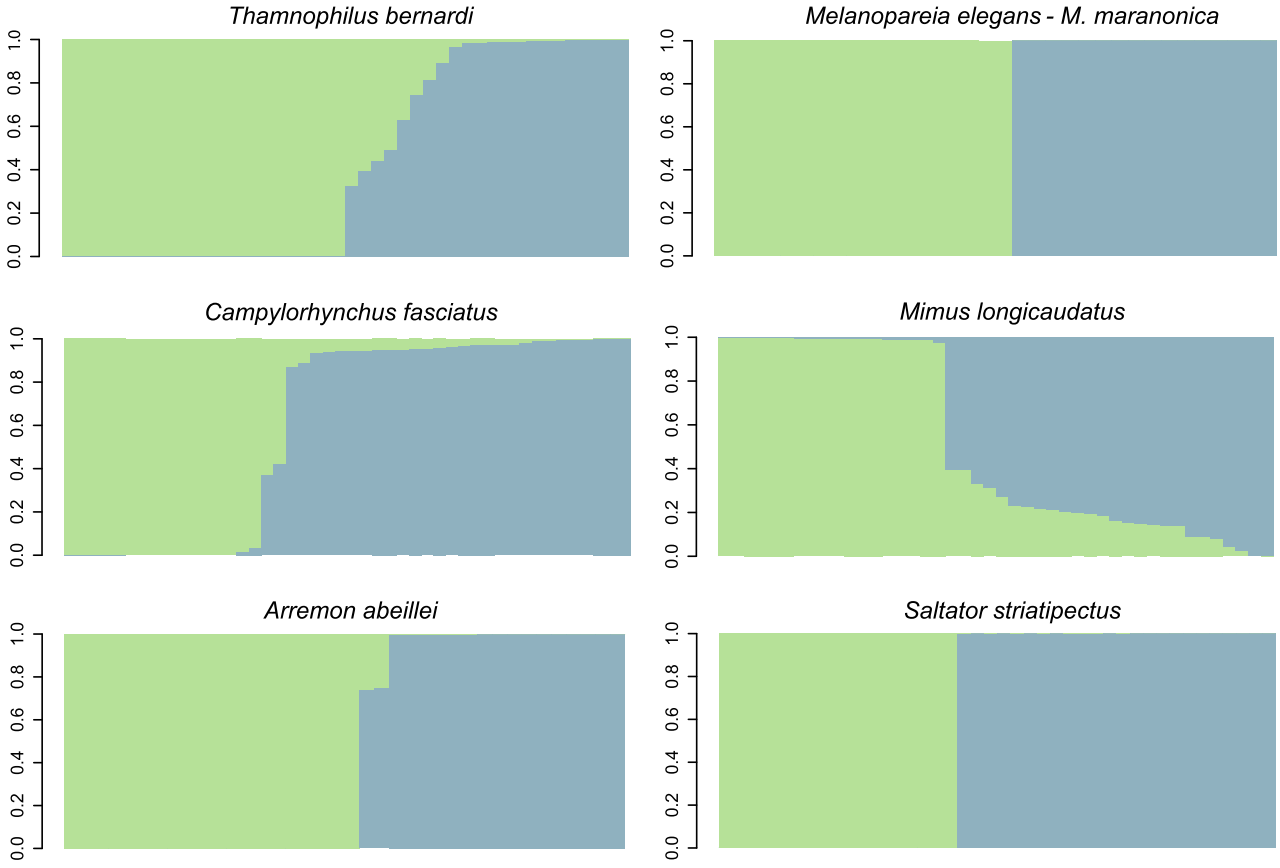

Fig. 2 STRUCTURE plots (K = 2) for each taxon pair showing assignment probability (y-axis) of each individual to Tumbes (green) and Marañón Valley (blue). Each bar represents an individual. Figure S2 (Supporting information) has the STRUCTURE plots with each bar labelled with collection locality, abbreviated species name and museum Accession no. [Colour figure can be viewed at wileyonlinelibrary.com]

isolation. Next, we found overall congruence in effective population size patterns that likely reflects that Tumbes and Marañón Valley had more expansive dry forests in the past, which is supported by Late Pleistocene fossil evidence near Tumbes (Oswald & Steadman 2015). Finally, we found congruence in the mode of population differentiation and inferred that the best-fit demographic model for all pairs was isolation with asymmetric gene flow. This result is not only important in showing the importance of gene flow during the diversification of these two bird faunas, but highlights a novel and general pattern of isolation with gene flow.

Concordant and discordant demographic history

We found similarity in the effective population sizes of the daughter and ancestral populations. Our estimates of ancestral population size are consistent with the prediction that arid-adapted taxa had larger ancestral population sizes historically when dry forest was more expansive in the region (Oswald & Steadman 2015). Based on estimates of N_e from our G-PhoCS analyses, all six pairs had larger ancestral populations than either of the daughter populations. However, the fastsimcoal2 analyses found that ancestral N_e was larger in only three of the pairs. In the remaining three pairs, the Tumbes and ancestral N_e values were similar or slightly smaller. Demographic congruence was also observed within the Marañón populations, which had smaller N_e than Tumbes populations. This demographic congruence likely reflects the smaller geographic area of the Marañón Valley in comparison with Tumbes. The higher genetic variation in Tumbes may also be due to more fragmented dry forests and arid habitats across a larger region relative to the Marañón Valley. These fragments could produce increased genetic structuring west of the Andes, although our sample size was too limited in geographic scope to detect it. Future fieldwork and sampling would further clarify the degree of genetic structuring among populations in Tumbes.

Model selection strongly favoured isolation with asymmetric gene flow from the Tumbes into the

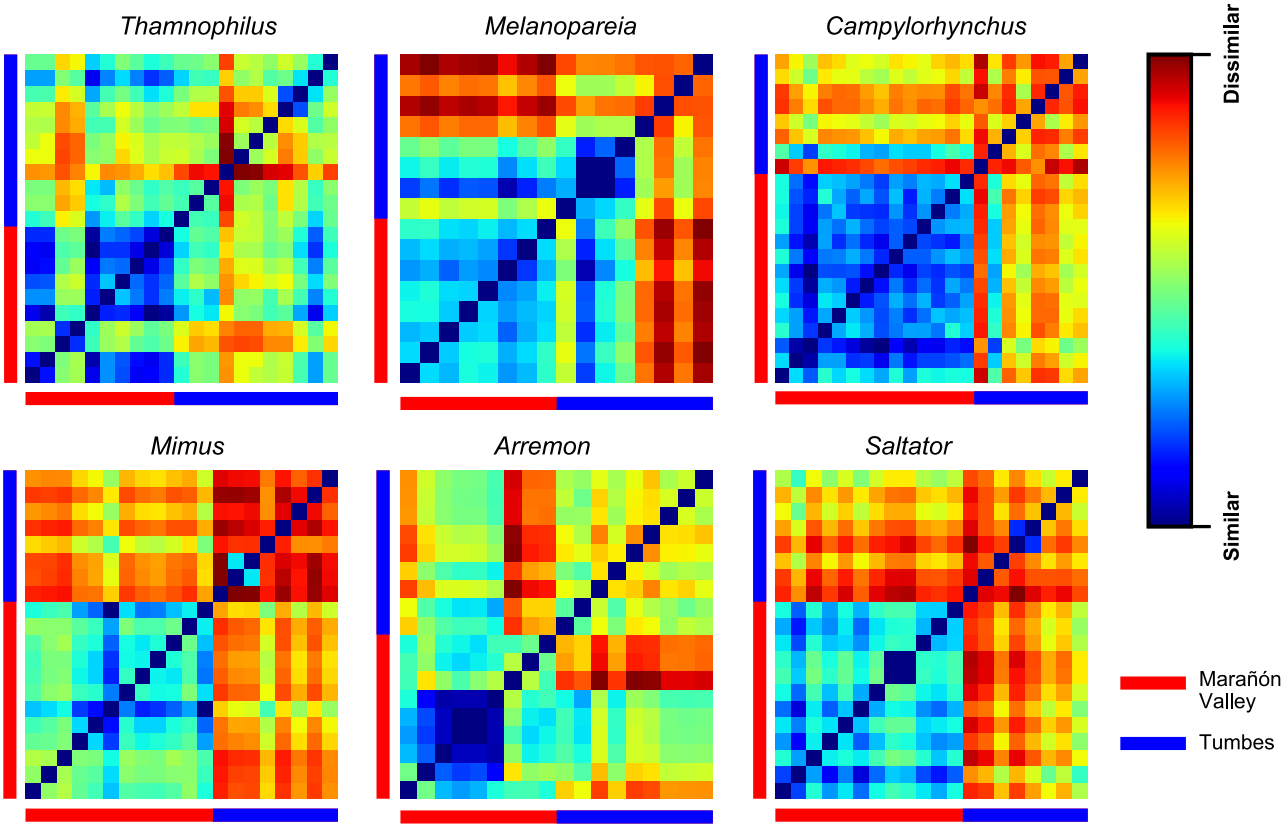

Fig. 3 Pairwise distance heatmap plots for each of the six taxon pairs. Warmer colours show individuals that are more genetically dissimilar and cooler colours show more similar individuals. Individuals from the Marañón Valley (red) and Tumbes (blue) are denoted with a coloured bar. [Colour figure can be viewed at wileyonlinelibrary.com]

Marañón Valley in all six taxon pairs. Speciation with gene flow is a well-described phenomenon that is documented in many systems (Nosil 2008), but, to our knowledge, the repeated cases of asymmetric gene flow that we observed are unique. This pattern is likely not the product of allopatric divergences followed by secondary contact with recent gene flow. All six taxon pairs are phenotypically different between the areas, which is the basis for their taxonomic classification as subspecies or species pairs, and there are no records of intermediate forms that would suggest contemporary hybridization or clinal variation. *Thamnophilus* is the only taxon pair in our data set in which the two populations may be coming into secondary contact in the Marañón Valley (Schulenberg *et al.* 2007), but hybrid phenotypes have not been documented. The relatively subtle phenotypic differences among each area likely reflect recent divergence between populations and the ecological similarity between the two areas. Our models indicate a high probability of gene flow after isolation, but it is unclear if this gene flow happened at the same time across species, for instance when a suitable habitat

Table 2 Population genetic summary statistics based on SNP data for the six focal taxon pairs occurring in the Marañón Valley and Tumbes

	n	π	H_O/H_E	θ_W	Taj. D
Marañón Valley					
Thamnophilus	10	0.002	0.148/0.128	0.004	−0.010
Melanopareia	8	0.003	0.076/0.098	0.004	0.198
Campylorhynchus	14	0.002	0.108/0.123	0.004	0.051
Mimus	13	0.002	0.010/0.124	0.004	−0.032
Arremon	9	0.004	0.088/0.114	0.006	0.253
Saltator	12	0.004	0.099/0.142	0.006	0.104
Tumbes					
Thamnophilus	12	0.003	0.184/0.229	0.004	−0.106
Melanopareia	9	0.005	0.132/0.176	0.006	0.081
Campylorhynchus	9	0.002	0.176/0.210	0.003	−0.015
Mimus	9	0.004	0.166/0.224	0.005	0.103
Arremon	10	0.006	0.121/0.194	0.007	0.097
Saltator	9	0.005	0.109/0.168	0.007	0.186

Column names are as follows: n, sample size; π, average nucleotide differences per site; H_O/H_E, observed and expected heterozygosity; θ_W, Watterson's Theta; and Taj. D, Tajima's D.

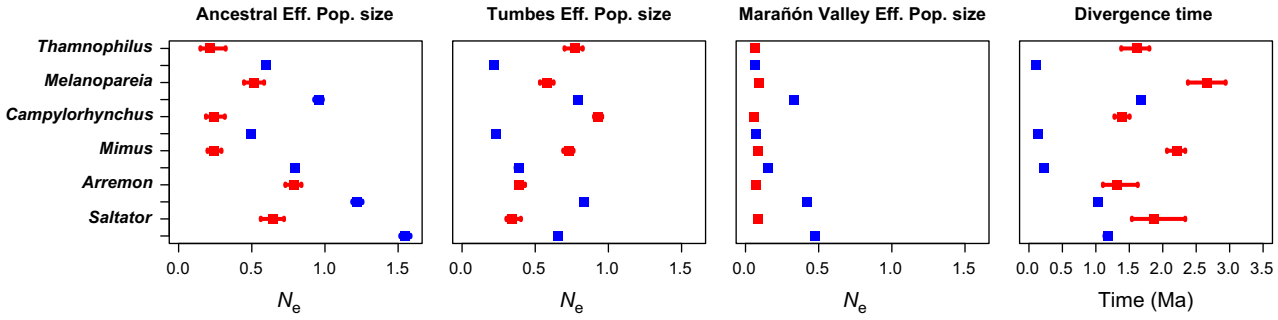

Fig. 4 Plots showing comparative demographic patterns from the six taxon pairs from fastsimcoal2 (red) and G-PhoCS (blue). From left to right: Ancestral N_e, Tumbes N_e, Marañón Valley N_e and divergence time of populations. N_e is in units of millions of individuals. *Y*-axis shows each of the taxon pairs. [Colour figure can be viewed at wileyonlinelibrary.com]

corridor existed (i.e. during glacial periods). The rate of gene flow varied across taxon pairs, but it was less than one migrant per generation, which in part explains how different phenotypes evolved in each area in the face of gene flow (Slatkin 1985, 1987). The generality of six repeated cases of isolation with asymmetric migration suggests that a shared factor that underlies the directionality of gene flow.

A general pattern of isolation with asymmetric gene flow is likely due to either more favourable dispersal conditions in one direction, differences in dispersal propensities and/or source-sink dynamics. There does not appear to be an extra physiological cost for dispersing in only one direction as is seen along elevational gradients in Andean birds (Cheviron & Brumfield 2009; DuBay & Witt 2014), because conditions should be the same in both directions. The asymmetry in size between Tumbes and the Marañón Valley could produce a source-sink dynamic where the higher number of individuals in Tumbes is more likely to disperse into the smaller geographic area of the Marañón Valley. El Niño events result in higher rainfall within Tumbes, leading to temporary mesic conditions and increased resource availability (Richter 2005; Muenchow *et al.* 2013). These dynamic conditions in Tumbes could lead to a higher dispersal propensity in birds, allowing them to track resources (Oswald *et al.* 2016). In contrast, the Marañón Valley is more climatically buffered from El Niño events because of the Andes (Bendix & Bendix 2006), leading to abiotic stability, which may cause populations to be more sedentary (Tripet *et al.* 2002; Salisbury *et al.* 2012). The underlying mechanism(s) influencing gene flow across northwestern Perú likely also acted in conjunction with Quaternary glacial–interglacial cycles that influenced the availability of suitable dispersal habitat in the region.

Our divergence time estimates between the Marañón Valley and Tumbes populations ranged widely (0.1–2.9 Ma), suggesting that a singular event was not responsible for the differentiation of the two bird faunas. Taking into account the uncertainty from both methods, the taxon pairs diverged in two (fastsimcoal2) to five (G-PhoCS) different time periods. These results also indicate that divergence most likely occurred after the final uplift of the Andes. Nonavian dry forest taxa typically have pre-Pleistocene divergences (Pennington *et al.* 2010; Werneck *et al.* 2012; Magalhaes *et al.* 2014), whereas most of the divergences in our data set postdate Andean uplift but pre-date the stronger and longer glacial cycles starting approximately 0.8 Ma (Lambeck *et al.* 2002). Pleistocene glacial–interglacial cycles likely had a repeated impact on the distribution and extent of dry forest in northwestern South America, but it is not apparent from our analysis that these cycles directly isolated populations. Alternatively, nonsimultaneous isolation could have happened via jump dispersal between the areas mediated by the dispersal ability of each species. Irrespective of the actual mechanism isolating these taxa, our results are consistent with other systems that show the historical assembly of Neotropical biotas is a protracted process (e.g. Smith *et al.* 2012).

Full- vs. composite-likelihood models

The coalescent methods fastsimcoal2 and G-PhoCS both offer flexible and powerful approaches for modelling demographic history, but we found clear differences that impact inferences in our study. We were able to analyse relatively large multilocus data sets and obtain stable parameter estimates in less than 8 weeks with both programmes. These findings were recovered in both the full- and composite-likelihood models we employed, but the full-likelihood approach typically had narrower uncertainty around parameter estimates. Among the important distinctions between the method outputs were that the fastsimcoal2 95% CIs from the parametric bootstrapping for divergence time were 7–23× wider than the 95% highest posterior density

Table 3 Demographic model selection results showing the likelihood of each model for each of the six taxon pairs. The models are as follows: M1 – Isolation with no migration; M2 – Isolation with symmetric migration; M3 – Isolation with asymmetric migration; M4 – Isolation with unidirectional migration, Marañón Valley to Tumbes; M5 – Isolation with unidirectional migration, Tumbes to Marañón Valley.

Thamnophilus	AIC	ΔAIC	Relative likelihood	AIC Weight
M1	17524.770	396.170	0.000	0.000
M2	17332.430	203.830	0.000	0.000
M3	17128.600	0.000	1.000	1.000
M4	17529.454	400.854	0.000	0.000
M5	17216.290	87.690	0.000	0.000
Melanopareia				
M1	33403.494	902.406	0.000	0.000
M2	32556.182	55.094	0.000	0.000
M3	32501.088	0.000	1.000	1.000
M4	33121.966	620.878	0.000	0.000
M5	33085.510	584.422	0.000	0.000
Campylorhynchus				
M1	16095.496	175.074	0.000	0.000
M2	16100.472	180.050	0.000	0.000
M3	15920.422	0.000	1.000	1.000
M4	16092.480	172.058	0.000	0.000
M5	15957.552	37.130	0.000	0.000
Mimus				
M1	24721.770	970.148	0.000	0.000
M2	24018.928	267.306	0.000	0.000
M3	23751.622	0.000	1.000	1.000
M4	24724.120	972.498	0.000	0.000
M5	23925.748	174.126	0.000	0.000
Arremon				
M1	24179.392	771.338	0.000	0.000
M2	23516.456	108.402	0.000	0.000
M3	23408.054	0.000	1.000	1.000
M4	24099.642	691.588	0.000	0.000
M5	23681.134	273.080	0.000	0.000
Saltator				
M1	42428.942	1147.446	0.000	0.000
M2	41404.602	123.106	0.000	0.000
M3	41281.496	0.000	1.000	1.000
M4	42116.736	835.240	0.000	0.000
M5	41858.786	577.290	0.000	0.000

(HPD) obtained from G-PhoCS posterior distributions (Fig. 4). The typically younger divergence times from G-PhoCS are likely linked to higher estimated ancestral N_e. In three cases, the fastsimcoal2 estimates were considerably older than the estimate from G-PhoCS. The uncertainty surrounding N_e estimates varied between the two approaches, with fastsimcoal2 population estimates being up to 3.3 times narrower for the Marañón Valley N_e 95% CIs. In contrast, the Tumbes and the ancestral N_e from G-PhoCS had up to 3.4 and 6.0 times narrower 95% HPD, respectively. As shown elsewhere (Gronau *et al.* 2011; Smith *et al.* 2014a), the migration estimates obtained from G-PhoCS are not robust to the prior and are used to obtain a more accurate estimate of divergence time, but not an accurate estimate of gene flow. In addition to being able to model migration rates, fastsimcoal2 provides a flexible means of comparing the likelihood of data under different demographic models, which is not possible in G-PhoCS. The ability to differentiate between varying demographic histories in this study provides an additional layer of inference not observable with even highly precise parameter estimates.

The trade-off between the precision of parameter estimates and model selection between the two software packages has important implications for phylogeographic inference. On one hand, precise parameter estimates provide increased resolution in coupling a genetic pattern to a hypothesized process responsible for the observed genetic variation. On the other hand, parameter estimates alone, irrespective of their uncertainty, do not provide an objective means of differentiating between alternative diversification scenarios (Carstens *et al.* 2009). By including demographic model selection, our study was able to capture an aspect of population history that is shared across six taxon pairs. If we had relied solely on divergence times, we would have concluded that the processes responsible for population isolation were entirely idiosyncratic, despite the fact that congruence in best-fit demographic models across the six taxon pairs indicates that the mode of population differentiation remained conserved over millions of years. It is unclear if the differences we obtained between G-PhoCS and fastsimcoal2 are unique to our data, but the distinction between precision in parameter estimates vs. the broad utility of demographic model selection for phylogeographic inference is general. There is a clear need moving forward, for model-based methods that can test the congruence in demographic histories in structured populations as has been developed for Sanger-based multilocus data (Huang *et al.* 2011) and unstructured populations using the aggregate site frequency spectrum (Xue & Hickerson 2015).

In sum, we used genome-wide genetic variation to model the population histories of bird species that are found in discontinuous dry forests in northwestern South America. We tested whether codistributed species showed similar patterns in the timing of isolation, effective population size and mode of diversification. Using a full-likelihood coalescent model, we inferred from sequence data that divergence times between taxon pairs occurring in the Tumbesian and Marañón Valley dry forests did not overlap. We used a complementary simulation-based approach and performed demographic model selection from the site frequency spectrum. Using this

method, we found strong support for a common diversification model of isolation with asymmetric gene flow between areas in all six taxon pairs. We further found congruence across species showing that ancestral population sizes were larger in the past and that contemporary population size patterns correlate with the geographic area of each dry forest. Our results highlight both the discordance in the absolute timing of diversification in co-distributed species and the congruence in demographic processes (i.e. genetic differentiation, asymmetric gene flow) that operate on different timescales.

Acknowledgements

For tissue samples, we thank LSUMNS (D. Dittmann, R. Brumfield, F. Sheldon), FLMNH (A. Kratter, D. Steadman), AMNH (P. Sweet, T. Trombone, J. Feinstein), UWBM (S. Birks, J. Klicka) and KU (M. Robbins, R. Moyle, T. Peterson). M. Hickerson, J. Satler, R. Terrill, Y. Momma, O. Johnson, A. Xue, G. Rosen, K. Provost, L. Moreira, G. Amato, M. Faiz, M. Gehara, M. Harvey, S. Robinson and P. Hosner kindly provided helpful feedback, support and discussion. We thank CORBIDI for logistical and field support in Peru. The New York Genome Center sequenced our samples. We also thank T. Särkinen kindly for providing a GIS layer of dry forest biomes used to make Fig. 1. We acknowledge and thank B. Carstens and two anonymous reviewers for giving helpful comments and feedback during the review process.

References

Avise JC (2000) *Phylogeography: The History and Formation of Species*. Harvard University Press, Cambridge, MA.

Bendix A, Bendix J (2006) Heavy rainfall episodes in Ecuador during El Nino events and associated regional atmospheric circulation and SST patterns. *Advances in Geosciences*, **6**, 43–49.

Bridgewater S, Pennington RT, Reynel CA, Daza A, Pennington TD (2003) A preliminary floristic and phytogeographic analysis of the woody flora of seasonally dry forest in northern Peru. *Candollea*, **58**, 129–148.

Burbrink F, Chan Y, Myers E, Ruane S, Smith BT, Hickerson M (2016) Asynchronous demographic responses to Pleistocene climate change in Eastern Nearctic vertebrates. *Ecology Letters*, **19**, 1457–1467.

Burham RJ, Graham A (1999) The history of Neotropical vegetation: new developments and status. *Annals of the Missouri Botanical Garden*, **86**, 546–589.

Burnham RJ (1995) A new species of winged fruit from the Miocene of Ecuador: *Tipuana ecuatoriana* (Leguminosae). *American Journal of Botany*, **82**, 1599–1607.

Burnham KP, Anderson DR (2003) *Model Selection and Multimodel Inference: A Practical Information-Theoretic Approach*. Springer Science & Business Media, New York, NY.

Burnham RJ, Carranco NL (2004) Miocene winged fruits of *Loxopterygium* (Anacardiaceae) from the Ecuadorian Andes. *American Journal of Botany*, **91**, 1767–1773.

Cadena CD, Pedraza CA, Brumfield RT (2016) Climate, habitat associations and the potential distributions of Neotropical birds: implications for diversification across the Andes. *La Revista de la Academia Colombiana de Ciencias Exactas, Físicas y Naturales*, **40**, 275–287.

Campbell KE Jr (1979) The non-passerine Pleistocene avifauna of the Talara Tar Seeps, Northwestern Peru. *Life Science Contributions of the Royal Ontario Museum*, **118**, 1–203.

Campbell KE Jr (1982) Late Pleistocene events along the coastal plain of Northwestern Peru. In: *Biological Diversity in the Tropics* (ed. Prance G). Columbia University Press, New York, NY.

Carstens BC, Stoute HN, Reid NM (2009) An information-theoretical approach to phylogeography. *Molecular Ecology*, **18**, 4270–4282.

Chaves JA, Hidalgo JR, Klicka J (2013) Biogeography and evolutionary history of the Neotropical genus Saltator (Aves: Thraupini). *Journal of Biogeography*, **40**, 2180–2190.

Cheviron ZA, Brumfield RT (2009) Migration-selection balance and local adaptation of mitochondrial haplotypes in Rufous-collared Sparrows (*Zonotrichia capensis*) along an elevational gradient. *Evolution*, **63**, 1593–1605.

Claramunt S, Cracraft J (2015) A new time tree reveals Earth history's imprint on the evolution of modern birds. *Science Advances*, **1**, e1501005.

Cohen MCL, Rossetti DF, Pessenda LCR, Friaes YS, Oliveira PE (2014) Late Pleistocene glacial forest of Humaitá. *Palaeogeography, Palaeoclimatology, Palaeoecology*, **425**, 37–47.

Colinvaux PA, De Oliveira PE, Moreno JE, Miller MC, Bush MB (1996) A long pollen record from lowland Amazonia: forest and cooling in glacial times. *Science*, **274**, 85–88.

Colinvaux PA, Bush MB, Steinitz-Kannan M, Miller MC (1997) Glacial and Postglacial Pollen Records from the Ecuadorian Andes and Amazon. *Quaternary Research*, **48**, 69–78.

Colinvaux PA, Oliveira PE, Bush MB (2000) Amazonian and Neotropical plant communities on glacial time-scales the failure of the aridity and refuge hypotheses. *Quaternary Science Reviews*, **19**, 141–169.

Core Team R (2014) *R: A Language and Environment for Statistical Computing*. R Foundation for Statistical Computing, Vienna.

DaCosta JM, Sorenson MD (2014) Amplification biases and consistent recovery of loci in a double-digest RAD-seq protocol. *PLoS ONE*, **9**, e106713.

DuBay SG, Witt CC (2014) Differential high-altitude adaptation and restricted gene flow across a mid-elevation hybrid zone in Andean tit-tyrant flycatchers. *Molecular Ecology*, **23**, 3551–3565.

Earl DA, vonHoldt BM (2012) STRUCTURE HARVESTER: a website and program for visualizing STRUCTURE output and implementing the Evanno method. *Conservation Genetics Resources*, **4**, 359–361.

Eaton DA (2014) PyRAD: assembly of de novo RADseq loci for phylogenetic analyses. *Bioinformatics*, **30**, 1844–1849.

Evanno G, Regnaut S, Goudet J (2005) Detecting the number of clusters of individuals using the software STRUCTURE: a simulation study. *Molecular Ecology*, **14**, 2611–2620.

Excoffier L, Dupanloup I, Huerta-Sánchez E, Sousa VC, Foll M (2013) Robust demographic inference from genomic and SNP data. *PLoS Genetics*, **9**, e1003905.

Falush D, van Dorp L, Lawson D (2016) A tutorial on how (not) to over-interpret STRUCTURE/ADMIXTURE bar plots. bioRxiv. Preprint.

Gronau I, Hubisz MJ, Gulko B, Danko CG, Siepel A (2011) Bayesian inference of ancient human demography from individual genome sequences. *Nature Genetics*, **43**, 1031–1034.

Gutenkunst RN, Hernandez RD, Williamson SH, Bustamante CD (2009) Inferring the joint demographic history of multiple populations from multidimensional SNP frequency data. *PLoS Genetics*, **5**, e1000695.

Hickerson MJ, Stahl EA, Lessios HA (2006) Test for simultaneous divergence using approximate Bayesian computation. *Evolution*, **60**, 2435–2453.

Hickerson MJ, Carstens BC, Cavender-Bares J *et al.* (2010) Phylogeography's past, present, and future: 10 years after. *Molecular Phylogenetics and Evolution*, **54**, 291–301.

Huang W, Takebayashi N, Qi Y, Hickerson MJ (2011) MTML-msBayes: approximate Bayesian comparative phylogeographic inference from multiple taxa and multiple loci with rate heterogeneity. *BMC Bioinformatics*, **12**, 1.

Jakobsson M, Rosenberg NA (2007) CLUMPP: a clustering matching and permutation program for dealing with label switching and multimodality in analysis of population structure. *Bioinformatics*, **23**, 1801–1806.

Lambeck K, Esat TM, Potter E-K (2002) Links between climate and sea levels for the past three million years. *Nature*, **419**, 199–206.

Lemon RH, Churcher CS (1961) Pleistocene geology and paleontology of the Talara Region, northwest Peru. *American Journal of Science*, **259**, 410–429.

Li H, Handsaker B, Wysoker A *et al.* (2009) The sequence alignment/map format and SAMtools. *Bioinformatics*, **25**, 2078–2079.

Linares-Palomino R (2006) Phytogeography and floristics of seasonally dry tropical forests in Peru. In: *Neotropical Savannas and Seasonally Dry Forests: Plant Diversity, Biogeography and Conservation* (eds Pennington RT, Lewis GP, Ratter JA), pp. 257–279. CRC Press, Boca Raton, FL.

Linares-Palomino R, Pennington RT, Bridgewater S (2003) The phytogeography of seasonally dry tropical forests in equatorial pacific South America. *Candollea*, **58**, 473–499.

Linares-Palomino R, Kvist LP, Aguirre-Mendoza Z, Gonzales-Inca C (2010) Diversity and endemism of woody plant species in the Equatorial Pacific seasonally dry forest. *Biodiversity Conservation*, **19**, 169–185.

Magalhaes ILF, Oliveira U, Santos FR, Vidigal THDA, Brescovit AD, Santos AJ (2014) Strong spatial structure, Pliocene diversification and cryptic diversity in the Neotropical dry forest spider *Sicarius cariri*. *Molecular Ecology*, **23**, 5323–5336.

Mayr E (1963) *Animal Species and Evolution*, vol. **797**. Belknap Press of Harvard University Press, Cambridge (MA).

McCormack JE, Hird SM, Zellmer AJ, Carstens BC, Brumfield RT (2013) Applications of next-generation sequencing to phylogeography and phylogenetics. *Molecular Phylogenetics and Evolution*, **66**, 526–538.

Miles A, Harding N (2016) scikit-allel: v0.20.3. Zenodo, 10.5281/zenodo.45420.

Muenchow J, von Wehrden H, Rodríguez EF, Rodrıguez RA, Bayer F, Richter M (2013) Woody vegetation of a Peruvian tropical dry forest along a climatic gradient depends more on soil than annual precipitation. *Erdkunde*, **67**, 241–248.

Myers EA, Hickerson MJ, Burbrink FT (2016) Asynchronous diversification of snakes in the North American warm deserts. *Journal of Biogeography*, **44**, 461–474.

Nam K, Mugal C, Nabholz B *et al.* (2010) Molecular evolution of genes in avian genomes. *Genome Biology*, **11**, R68.

Nosil P (2008) Speciation with gene flow could be common. *Molecular Ecology*, **17**, 2103–2106.

Oswald JA, Steadman DW (2015) The changing diversity and distributions of dry forest passerine birds in northwestern Peru since the last ice age. *The Auk*, **132**, 836–862.

Oswald JA, Burleigh JG, Steadman DW, Robinson SK, Kratter AW (2016) Historical climatic variability and geographical barriers as drivers of community composition in a biodiversity hotspot. *Journal of Biogeography*, **43**, 123–133.

Parker III TA, Schulenberg TS, Kessler M, Wust WW (1995) Natural history and conservation of the endemic avifauna in north-west Peru. *Bird Conservation International*, **5**, 201–213.

Pennington RT, Prado DE, Pendry CA (2000) Neotropical seasonally dry forest and quaternary vegetation changes. *Journal of Biogeography*, **27**, 261–273.

Pennington RT, Ratter JA, Lewis GP (2006) An overview of the plant diversity, biogeography and conservation of Neotropical savannas and seasonally dry forests. In: *Neotropical Savannas and Seasonally Dry Forests: Plant Diversity, Biogeography and Conservation* (eds Pennington RT, Lewis GP, Ratter JA), pp. 1–29. CRC Press, Boca Raton, FL.

Pennington RT, Lavin M, Oliveira-Filho A (2009) Woody plant diversity, evolution, and ecology in the tropics: perspectives from seasonally dry tropical forests. *Annual Review of Ecology, Evolution, and Systematics*, **40**, 437–457.

Pennington RT, Lavin M, Särkinen T, Lewis GP, Klitgaard BB, Hughes CE (2010) Contrasting plant diversification histories within the Andean biodiversity hotspot. *Proceedings of the National Academy of Sciences of the United States of America*, **107**, 13783–13787.

Peterson BK, Weber JN, Kay EH, Fisher HS, Hoekstra HE (2012) Double digest RADseq: an inexpensive method for de novo SNP discovery and genotyping in model and non-model species. *PLoS ONE*, **7**, e37135.

Pinho C, Hey J (2010) Divergence with gene flow: models and data. *Annual Review of Ecology, Evolution, and Systematics*, **41**, 215–230.

Prates I, Xue AT, Brown JL *et al.* (2016) Inferring responses to climate dynamics from historical demography in neotropical forest lizards. *Proceedings of the National Academy of Sciences*, **113**, 7978–7985.

Pritchard JK, Stephens M, Donnelly P (2000) Inference of population structure using multilocus genotype data. *Genetics*, **155**, 945–959.

Rambaut A, Drummond AJ (2010) *TRACER Version 1.5*. Oxford University Press, Oxford.

Rannala B, Yang Z (2003) Bayes estimation of species divergence times and ancestral population sizes using DNA sequences from multiple loci. *Genetics*, **164**, 1645–1656.

Richter M (2005) Vegetation development before, during, and after El Niño 1997/98 in Northwestern Peru. *Lyonia*, **8**, 19–27.

Salisbury CL, Seddon N, Cooney CR, Tobias JA (2012) The latitudinal gradient in dispersal constraints: ecological specialisation drives diversification in tropical birds. *Ecology Letters*, **15**, 847–855.

Särkinen T, Iganci JRV, Linares-Palomino R, Simon MF, Prado DE (2011) Forgotten forests - issues and prospects in biome mapping using Seasonally Dry Tropical Forests as a case study. *BMC Ecology*, **11**, 27.

Särkinen T, Pennington RT, Lavin M, Simon MF, Hughes CE (2012) Evolutionary islands in the Andes: persistence and isolation explain high endemism in Andean dry tropical forest. *Journal of Biogeography*, **39**, 884–900.

Satler JD, Carstens BC (2016) Phylogeographic concordance factors quantify phylogeographic congruence among co-distributed species in the *Sarracenia alata* pitcher plant system. *Evolution*, **70**, 1105–1119.

Schulenberg TS, Stotz DF, Lane DF, O'Neill JP, Parker TA III (2007) *Birds of Peru*. Princeton University Press, Princeton (NJ).

Slatkin M (1985) Gene flow in natural populations. *Annual Review of Ecology and Systematics*, **16**, 393–430.

Slatkin M (1987) Gene flow and the geographic structure of natural populations. *Science*, **236**, 787–792.

Smith BT, Amei A, Klicka J (2012) Evaluating the role of contracting and expanding rainforest in initiating cycles of speciation across the Isthmus of Panama. *Proceedings of the Royal Society B*, **279**, 3520–3526.

Smith BT, Harvey MG, Faircloth BC, Glenn TC, Brumfield RT (2014a) Target capture and massively parallel sequencing of ultraconserved elements for comparative studies at shallow evolutionary time scales. *Systematic Biology*, **63**, 83–95.

Smith BT, McCormack JE, Cuervo AM *et al.* (2014b) The drivers of tropical speciation. *Nature*, **515**, 406–409.

Stattersfield AJ, Crosby MJ, Long AJ, Wege DC(1998) Endemic Bird Areas of the World. Priorities for biodiversity conservation. BirdLife Conservation Series 7. BirdLife International, Cambridge, United Kingdom.

Stotz DF, Fitzpatrick JW, Parker TA III, Moskovits DK (1996) *Neotropical Birds: Ecology and Conservation*. The University of Chicago Press, Chicago, IL.

Tripet F, Christe P, Møller AP (2002) The importance of host spatial distribution for parasite specialisation and speciation: comparative study of bird leas (Siphonaptera: Ceratophyllidae). *Journal of Animal Ecology*, **71**, 735–748.

Weigend M (2002) *Additional observations on the biogeography of the Amotape-Huancabamba zone in Northern Peru: defining the South-Eastern limits Revista Peruana de Biología*, **11**, 127–134.

Werneck FP, Gamble T, Colli GR, Rodrigues MT, Sites JW Jr (2012) Deep diversification and long-term persistence in the South American 'dry diagonal': integrating continent-wide phylogeography and distribution modeling of geckos. *Evolution*, **66**, 3014–3034.

Xue AT, Hickerson MJ (2015) The aggregate site frequency spectrum for comparative population genomic inference. *Molecular Ecology*, **24**, 6223–6240.

Yang Z (2002) Likelihood and Bayes estimation of ancestral population sizes in hominoids using data from multiple loci. *Genetics*, **162**, 1811–1823.

All authors assisted in writing the manuscript. J.A.O. led the writing of the manuscript, collected specimens and conceived the project; I.O. developed methods, assisted in data analysis and design; W.M.M. III assisted with data collection in the laboratory and project design; M.J.A. assisted with data collection in the laboratory and project design; B.T.S. conceived the project, assisted in data analysis and design, contributed substantial materials and resources, and led the writing of the manuscript.

Data accessibility

Raw sequence read data are available from the NCBI Sequence Read Archive, Bioproject PRJNA355591. Bio Sample Accession nos: SAMN06090171–SAMN06090296. G-PhoCS, fastsimcoal2 and STRUCTURE input files are available from DRYAD (https://datadryad.org/; doi:10.5061/dryad.6k630.

Supporting information

Additional supporting information may be found in the online version of this article.

Fig. S1 Plot of *dd*RAD reads from each species mapped to the Zebra finch (*Taeniopygia guttata*) genome. On the *Y*-axis are chromosomes 1–28, Z sex chromosome, the mitochondrial genome (MT), and unmapped (Un). The X axis shows the percentage of the reads that mapped to the chromosome relative to the total size of the genome. The percentage size of each chromosome is shown in black. The taxon pairs are as follows: *Arremon* (aqua), *Campylorhynchus* (maroon), *Melanopareia* (dark yellow), *Mimus* (red), *Saltator* (green), and *Thamnophilus* (blue).

Fig. S2 STRUCTURE plots (K = 2), with sample IDs, for each taxon pair showing assignment probability (*y*-axis) of each individual to Tumbes (green) and Marañón Valley (blue). Each plot has the focal genus name as a title with each individual represented below the bar. The individual name begins with 'Tum' or 'Mar', which indicates that that individual was collected in Tumbes or the Marañón Valley, respectively. Labels end with the shortened scientific name. ThaBer = *Thamnophilus bernardi*, MelEle = *Melanopareia elegans*, MelMar = *Melanopareia maranonica*, CamFas = *Campylorhynchus fasicatus*, MimLon = *Mimus longicaudatus*, ArrAbe = *Arremon abeillei*, SalStr = *Saltator striatipectus*. Shortened scientific names are followed by the museum accession number. More detailed collecting localities and museum information can be found in Table S1.

Fig. S3 Alternative STRUCTURE plots for taxon pair that have K = 3 as the most likely model. Each bar represents an individual, and the *y*-axis shows the assignment probability of each individual to the three populations (K). The individual name begins with 'Tum' or 'Mar', which indicates that that individual was collected in Tumbes or the Marañón Valley, respectively. Labels end with the shortened scientific name. ThaBer = *Thamnophilus bernardi*, CamFas = *Campylorhynchus fasicatus*, and SalStr = *Saltator striatipectus*. Shortened scientific names are followed by the museum accession number.

Table S1 Museum accession numbers and locality information for specimens. Museum abbreviations are as follows: LSUMZ = Louisiana State University Museum of Natural Science, FLMNH = Florida Museum of Natural History, UWBM = Burke Museum, KU = University of Kansas Biodiversity Institute, AMNH = American Museum of Natural History.

Table S2 STRUCTURE output from Structure Harvester for each focal taxon pair including the Number of populations (K), Number of replicates, Mean log-likelihood score, Log-likelihood standard deviation (SD), First- and Second-order likelihood rate of change, and ΔK value.

Table S3 Demographic modeling output from fastsimcoal2 and G-PhoCS. The top table shows fastsimcoal2 model for the best-fit model (isolation with asymmetric gene flow) output with maximum likelihood estimates, and mean and 95% confidence intervals from 50 bootstrap replicates for: ancestral, Marañón Valley, and Tumbes N_e; migration rates from Marañón Valley to Tumbes and Tumbes to Marañón Valley; and divergence time between Marañón Valley and Tumbes. The middle table shows the G-PhoCS output for the isolation model with gene flow using prior 1 (τ–θ: ([1, 300]) with mean and the highest posterior density for: ancestral, Marañón Valley, and Tumbes N_e; migration rates from Marañón Valley to Tumbes and Tumbes to Marañón Valley; and divergence time between Marañón Valley and Tumbes. The bottom table shows the G-PhoCS output for the pure isolation model using prior 1 with mean and the highest posterior density for: ancestral, Marañón Valley, and Tumbes N_e; and divergence time between Marañón Valley and Tumbes.